Reduction of background scattered light in vacuum systems for cold atoms experiments

Vovrosh, J.; Earl, L.; Thomas, H.; Winch, J.; Stray, B.; Ridley, K.; Langlois, M.; Bongs, K.; Holynski, M.

DOI:
10.1063/5.0030041

Reduction of background scattered light in vacuum systems for cold atoms experiments

Cite as: AIP Advances **10**, 105125 (2020); https://doi.org/10.1063/5.0030041
Submitted: 18 September 2020 . Accepted: 30 September 2020 . Published Online: 20 October 2020

J. Vovrosh, L. Earl, H. Thomas, J. Winch, B. Stray, K. Ridley, M. Langlois, K. Bongs, M. Holynski, et al.

Reduction of background scattered light in vacuum systems for cold atoms experiments

Cite as: AIP Advances 10, 105125 (2020); doi: 10.1063/5.0030041
Submitted: 18 September 2020 • Accepted: 30 September 2020 •
Published Online: 20 October 2020

J. Vovrosh, L. Earl, H. Thomas, J. Winch, B. Stray, K. Ridley, M. Langlois, K. Bongs, and M. Holynski[a)]

AFFILIATIONS

Midlands Ultracold Atom Research Center, School of Physics and Astronomy, University of Birmingham, Birmingham B15 2TT, United Kingdom

[a)]Author to whom correspondence should be addressed: M.Holynski@bham.ac.uk

ABSTRACT

Recent advances in the understanding and control of cold atom systems have resulted in devices with extraordinary metrological performance. To further improve the performance in these systems, additional methods of noise reduction are needed. Here, we examine the noise reduction possible from vacuum compatible low reflection coatings in cold atom systems by characterizing a black coating and its compatibility in a Magneto-Optical Trap (MOT). We demonstrate that the commercially available PCO35® coating provides low-reflectivity surfaces that are ultra-high vacuum compatible. The reflective properties of the coating are compared to titanium, a common vacuum chamber material, and the reduction to scattered light is characterized over a range of angles and wavelengths. The outgassing properties of the coating are measured to be less than that of the vacuum system used to test the coating, which is limited to 3×10^{-8} mbar L cm^{-2} s^{-1}. The coating is applied to a vacuum chamber housing a rubidium prism MOT, and its vacuum compatibility is assessed and compared to an identical non-coated system. Finally, the effect of scattered light reduction in a generalized system is explored theoretically. These results show promise for reducing background light in cold atom experiments via the use of low-reflectivity coatings.

I. INTRODUCTION

The exceptional performance of cold atom systems has enabled measurements of the fine structure constant,[1] the equivalence principle,[2] the gravitational constant,[3] and the redefinition of the kilogram as part of a watt balance[4] and resulted in several proposals for gravitational wave detection.[5–7] In addition, quantum technologies based on cold atoms have begun to move out of the lab and into the real world, where they are expected to address a number of different applications.[8–10] Despite this success, there is still scope to make these devices more sensitive and for even more precise measurements to be made.

In a cold atom system, one or more photodetectors are often used to measure light produced by atom fluorescence. Fluctuations in the photodetector signal limit the accuracy of the measurement. There are a number of different sources of fluctuations: atom shot noise (also known as quantum projection noise), shot noise associated with signal and background photons, shot noise on the photodetector dark current, and thermal noise in the photodetector amplifier circuits (Johnson noise). Often, measurements are taken where the background light level is subtracted; shot noise fluctuations will cause an increase in the noise when this subtraction is performed. Background light in cold atom systems often originates from specular reflections off of vacuum chamber walls and fluorescence from background atoms. These effects have been observed to introduce systematic shifts and noise sources, as well as loss of contrast in many cold atom systems including gyroscopes,[11,12] clocks,[13] and gradiometers.[14] Reducing these noise sources will be particularly important when realizing current proposals for cold atom experiments targeting fundamental physics.[15,16] Reducing these noise sources is also important for maximizing the sensitivity of portable cold atom sensors utilizing single beam geometries[17] due to the high level of light scattered in these systems.[18,19]

The noise arising from scattered laser light can seriously reduce the signal-to-background and signal-to-noise ratios in detection. To suppress unwanted scattered light, blackened surfaces are often used.[20–23] Each black coating has different properties, including varying absorption with wavelength,[22,23] ability to be applied to specific materials, reactivity with certain chemicals, and different levels

of vacuum compatibility.[24–26] The variation in properties between different blackened coatings makes some coatings better suited for some applications than others.[23]

Here, we assess the improvements that in-vacuum anti-reflection coatings can offer in terms of reducing noise in cold atom systems and provide the theoretical tools to allow for the expected benefits to be calculated. To do this, we evaluate a coating's suitability in terms of its optical properties, for a number of commonly used wavelengths, and pressure regimes typically used in cold atom systems. We then test the properties of the coating in a Magneto-Optical Trap (MOT), a sub-component that is common to most cold atom systems, in which we test the chemical compatibility of the coating with rubidium. We then evaluate the reduction in noise from background scatter and use this to estimate the theoretical improvements to a generalized cold atom sensor. The tests and theory presented provide a tool set to allow for the potential benefits of low-reflectivity coatings in existing systems to be evaluated.

II. CHARACTERIZATION OF OPTICAL PROPERTIES

While there are several commercial coatings available, which potentially could be used, the commercially available PCO35®[27] coating has been chosen. The coating is ceramic-like and can be produced on anodically contacted substrate materials, including aluminum, titanium, and magnesium alloys.[27] An example of a coated part can be seen in Fig. 1.

In cold atom systems, background light typically is the result of light scattered multiple times from different vacuum surfaces and angles. When attempting to eliminate background light, the relative positions of the light source, scattering surface, and detector significantly affect the relative intensity of scattered light. Surfaces typically have very different reflectance properties between near normal incidence and near grazing incidence; therefore, optical reflectance is normally described using the bidirectional reflectance distribution function[24,28] (BRDF) $f_r(\theta_i, \theta_r, \phi_r)$, given by

$$f_r(\theta_i, \theta_r, \phi_r) = \frac{P_r D^2}{P_i A \cos(\theta_r)}, \quad (1)$$

where P_r is the reflected laser power, D is the distance between the sample and the detector, P_i is the incident power on the sample, A is the area of the detector, θ_i is the angle of incident light, and θ_r is the reflected polar angle [see Fig. 2(a)].

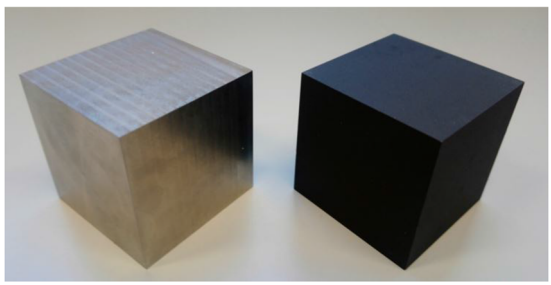

FIG. 1. Titanium cube (left) and coated titanium cube (right).

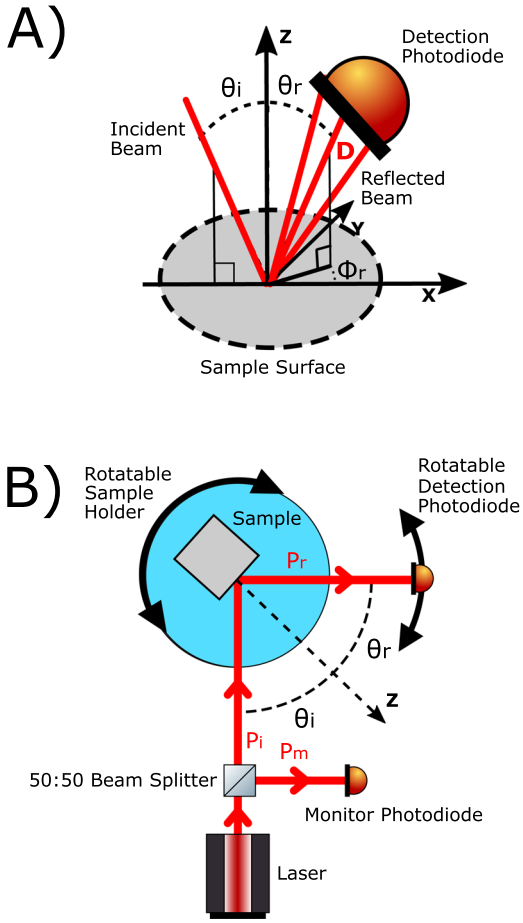

FIG. 2. The experimental setup for testing the optical properties of the coating. (a) The coordinate system used for the measurements. The z-axis is the surface normal. The incident light travels in the x–z plane at angle θ_i to the normal. Reflected light is measured at polar angle θ_r and azimuthal angle ϕ_r on a detector of area A with distance D away. (b) The experimental setup used to measure the BRDF distribution of the samples.

To characterize the reflectance from the samples, shown in Fig. 1, a laser beam with a $1/e^2$ beam waist of 0.37 mm was shone incident on the surface, perpendicular to the axis of rotation of a turntable sample holder. Both the sample and the detection photodiode could be rotated independently about the rotation axis. The reflected power P_r is measured on the detection photodiode. A 50:50 beam splitter cube is used to split off an amount of light to monitor the laser power P_m incident on the sample, allowing for any laser source intensity fluctuations to be accounted for. The reflected intensity was measured by a photodiode that could be rotated independently around the axis. The experimental setup can be seen in Fig. 2(b).

The BRDF results can be seen in Fig. 3. In Fig. 3(b), compared to an uncoated titanium cube, the amount of light reflected at peak reflection was reduced by a factor of 62. Optical measurements were taken again after ultrasonic cleaning of the sample. This was done to identify if the cleaning procedure for ultra-high

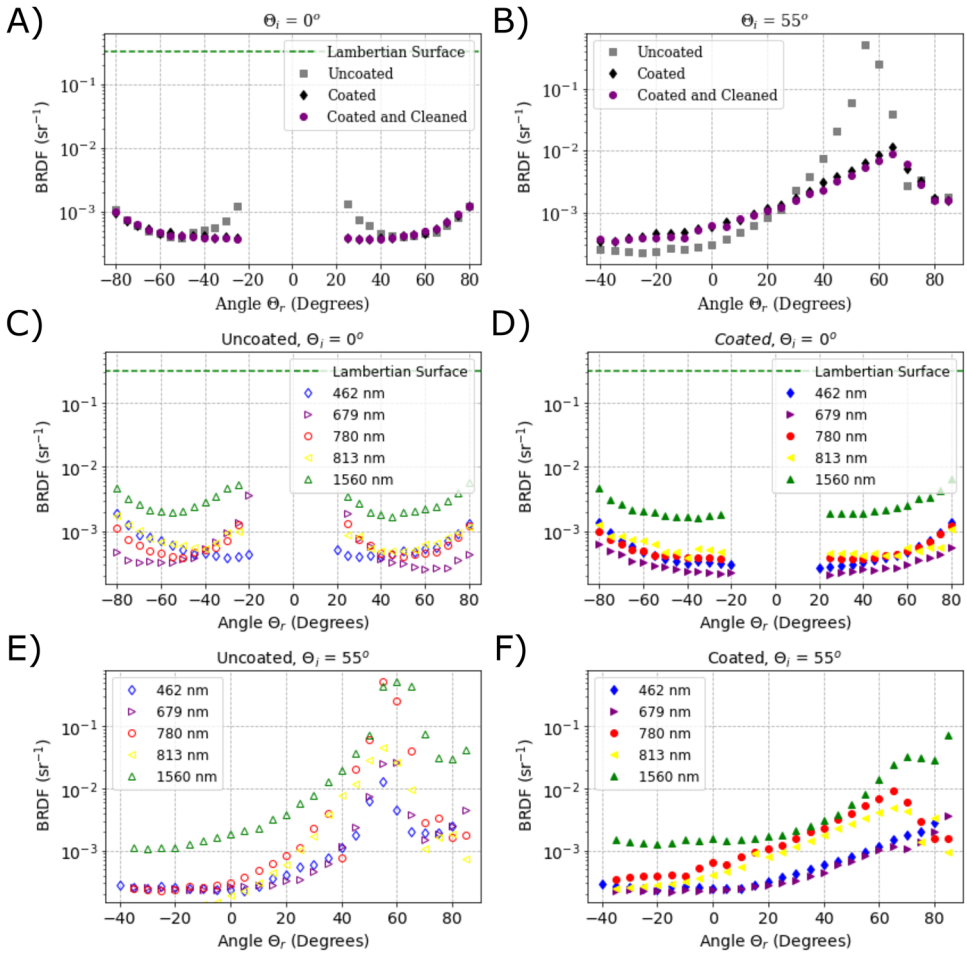

FIG. 3. Bidirectional reflection distribution function (BRDF) vs reflection angle. The dashed line represents a Lambertian surface with unit reflectivity. (a) A comparison of the uncoated and coated titanium block at $\lambda = 780$ nm at normal incidence ($\theta_i = 0°$). (b) A comparison of the uncoated and coated titanium block at $\lambda = 780$ nm at $\theta_i = 55°$. The coated and uncoated titanium block was tested for a variety of commonly used wavelengths in cold atom physics at (c) uncoated at normal incidence ($\theta_i = 0°$), (d) coated at normal incidence ($\theta_i = 0°$), (e) uncoated at $\theta_i = 55°$, and (f) coated at $\theta_i = 55°$. The error on the BRDF measurements is less than 13% of the measured value in all cases, and the error in the accuracy of θ_r is ±0.5°.

vacuum (UHV) would affect the optical properties. It can be seen in Figs. 3(a) and 3(b) that the coated sample showed negligible difference in its optical properties, suggesting that the optical performance of the coating will not be reduced when preparing it for vacuum applications.

The BRDF properties of titanium both coated and uncoated were also measured at a number of commonly used wavelengths. The results of this can be found in Fig. 3, with [(c) and (e)] showing the results from the uncoated cube and [(d) and (f)] showing the results from the coated cube. It can be seen that the performance of the coating varies with wavelength. The biggest reduction in the total scattered light occurred at 780 nm and the smallest amount occurred at 462 nm. Despite the variation in the BRDF with wavelength, the BRDF remains lower than the uncoated sample for all wavelengths examined. This should allow for this coating to be used in a variety of experiments that require different wavelengths.

For all of the results taken with light incident on the sample at 55° in Fig. 3, it can be seen that the BRDF profile is not only reduced in amplitude but broadened and shifted, which is to be expected for certain complex surface structures.[29,30]

III. CHARACTERIZATION OF VACUUM PROPERTIES

To ensure that the coating is suitable for the high vacuum conditions in which cold atom systems operate, it is vital that the outgassing rate of the coating is low, ideally no higher than that of the materials normally used to make vacuum systems. Before the coated cube was placed into the vacuum chamber, it was cleaned using a procedure adapted from the CERN cleaning guidelines.[31]

The cleaned and coated cube was placed in a room-temperature vacuum chamber, which was then brought to UHV by a turbo pump, backed by a dry rotary roughing pump. A bakeout was performed

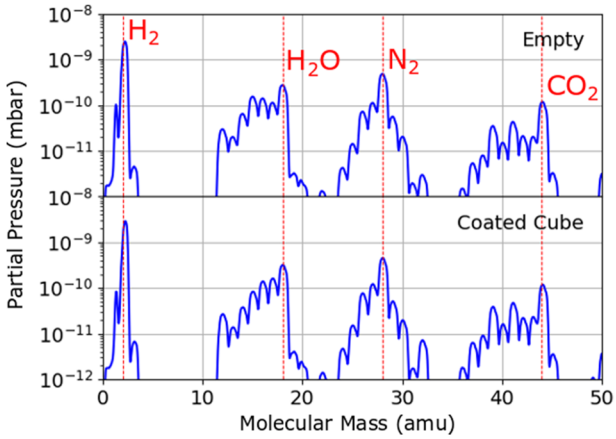

FIG. 4. Residual gas analysis of materials in a vacuum system 24 h after cleaning and bakeout processes. The top curve is the residual gas of an empty chamber and the bottom curve is of the same chamber with the coated cube in. There are no increases in excess water or complex hydrocarbons in the range measured.

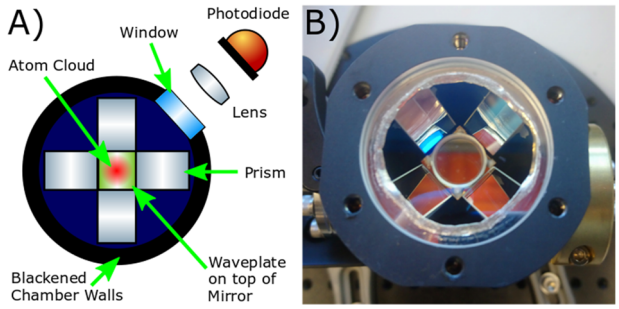

FIG. 5. The coated science chamber. (a) Schematic of the vacuum chamber internals and detection system. The window used for detection is located between the prisms. The light that passes through this window is focused by a 12 mm diameter lens onto a photodiode. The total light detection efficiency of the system is 0.3%. (This includes losses due to the geometry, optical losses, and the photodiode's quantum efficiency.) The lens and the vacuum window are both coated with an anti-reflection coating at 780 nm. (b) Top down photo of the coated vacuum chamber showing the 10 mm prisms used to form a MOT.

for 72 h at a maximum temperature of 130 °C, limited with the use of indium seals. The coating itself is resistant against constant temperatures up to 423 K.[27] Temperature ramping during bakeout was limited to 5 °C/h. UHV was maintained using an ion pump, and a residual gas analyzer (RGA) was employed to measure the remaining components. The vacuum chamber, both when empty and with a sample inside, was able to be pumped to an ultimate pressure of 2×10^{-9} mbar. The outgassing rates of the vacuum system with and without the coated sample were measured via the pressure rate of rise curves.[32] The outgassing rate was found to be $3 \pm 0.3 \times 10^{-8}$ mbar L cm^2 s^{-1} for the empty chamber and $2 \pm 0.3 \times 10^{-8}$ mbar L cm^2 s^{-1} with the coated cube inside, suggesting that the outgassing rate of the coating is less than that which is resolvable with this experimental system.

To characterize the specific elements outgassing from the coating, the residual gas properties of the chamber were measured with and without the coated sample. When the residual gas analyzer (RGA) was turned on, the pressure rose to 3.5×10^{-8} mbar. This behavior is typical in hot-filament vacuum gauges, such as an RGA, due to absorption processes.[33] The results of the measurements can be seen in Fig. 4.

Figure 4 shows that the spectrum of residual gases present in the chamber with and without the coated cube is very similar. This suggests that the coating in the range examined will not introduce a particularly sharp increase in any one element of the vacuum chamber. From the measurements taken here, and within the limits of the vacuum system used to test the vacuum properties of the coated cube, it can be seen that the outgassing properties of the coating were not an issue at pressures on the order of 10^{-9} mbar and no large amounts of elements that react with rubidium are emitted by the coating. These results show that the coating can be used at pressures relevant to cold atom systems.[11–14]

IV. PERFORMANCE IN A COLD ATOM SYSTEM

Since the field of cold atoms uses primarily reactive elements, the coating was tested in a rubidium prism MOT to verify compatibility with vacuum cleaning methods, baking, and use with rubidium.[34] A titanium science chamber housing a prism MOT, identical to that previously reported,[10] was constructed with the coating applied before vacuum assembly. Once assembled, the system was baked out at 100 °C for ~ 70 h. After baking, the pressure was maintained with a 2 l s^{-1} ion pump, and the ultimate pressure of the system achieved was of the order 10^{-9} mbar, prior to dispenser activation. The coated and assembled science chamber can be seen in Fig. 5. A single input beam is shone directly into the vacuum chamber in which the four prisms, a quarter wave plate, and a mirror are used to create the six counter propagating beams required to cool the atoms in all three degrees of freedom. A pair of coils were used to create a quadrupole field magnetic field with a linear gradient, which has zero field at the center of the trapping region.

A fiber laser system[10] was used to shine a circularly polarized 30 mm $1/e^2$ diameter laser beam of equal power (14.6 mW) incident on both the coated and uncoated chamber. Atoms were cooled and trapped in a prism MOT,[35] loaded from background atomic vapor that was produced under vacuum raising the pressure in the vacuum. The scattered light was measured through a side window and focused onto a photodiode. In the uncoated chamber, a cloud of $4 \pm 0.6 \times 10^7$ atoms was measured with a loading time of 0.9340 ± 0.0001 s at a vacuum pressure of 8.6×10^{-7} mbar. In the coated chamber, a cloud of $6 \pm 0.9 \times 10^7$ atoms was measured with a loading time of 1.130 ± 0.003 s at a vacuum pressure of 9.5×10^{-7} mbar. It can be seen that there is no negative measurable effect from the coating on the atom number or loading time. After performing the measurements and turning off the dispensers used to create the background atomic vapor, the pressure in the vacuum chambers returned to their previous values.

The vacuum chamber has been heat cycled three times without any noticeable degradation to the coating performance, and since its construction, the chamber has shown vacuum stability for over one month with no obvious abnormalities occurring, suggesting that the coating has not reacted with rubidium or deteriorated during this time.

As well as measuring scattered light from the MOT, the quadrupole field coils were turned off and incident light was switched between being on and off resonant with the ^{87}Rb cooling transition. This was done to measure the scattered light contribution from the chamber and any background fluorescence from the atoms. The coated chamber saw a reduction in background light by 40% ± 4%. While the results shown here demonstrate a significant improvement, it should be noted that the in-vacuum prisms are responsible for a lot of scattered light seen within the chamber. However, for many other cold atom systems, such as six beam MOTs,[36] this will not be a limiting factor.

V. REDUCTION OF BACKGROUND LIGHT IN A GENERALIZED COLD ATOM SYSTEM

To consider the potential impact on cold atom systems, we consider an experimental setup in which fluorescence imaging of an atom cloud onto a photodiode is performed for the purpose of measuring the number of atoms in the cloud. In this case, we assume an optimized system where background light has been measured and subtracted from the signal of interest so that the only effect of the background light is additional shot noise on the photodiode output. All the noise sources, including shot noise from the background light, can be quantified by their variances, and a total noise figure can be obtained by combining the noise sources in quadrature, i.e., adding the variances. Let σ_b be the standard deviation (the square root of the variance) of the photocurrent due to shot noise on the background light. This quantity is proportional to the square root of the power of the background light incident on the photodetector,[37]

$$\sigma_b = \sqrt{2eRP_b\Delta v}, \tag{2}$$

where R is the detector responsivity in A/W, e is the charge on the electron, P_b is the optical power in Watts, and Δv is a bandwidth factor. Let the standard deviation of all the other noise sources combined be σ_1. The standard deviation including background light, σ_2, is, therefore, given by

$$\sigma_2 = \sqrt{\sigma_1^2 + \sigma_b^2}. \tag{3}$$

The aim of coating the vacuum chamber is to reduce the value of P_b and, thus, reduce the value of σ_2, which will improve the overall signal-to-noise ratio (SNR) in inverse proportion to the reduction in σ_2. For a given reduction in P_b, the amount by which σ_2 is reduced depends on how large σ_b is relative to σ_1; that is, how significant the background light is as a source of noise relative to all the other noise sources. Suppose the coating changes the level of background light P_b by factor Y, where $Y = 1$ is equivalent to no reduction and $Y = 0$ is a complete reduction in background light. A reduction by factor Y affects σ_2 by factor F. Using Eqs. (2) and (3) gives

$$F = \sqrt{\frac{1 + YX^2}{1 + X^2}}, \tag{4}$$

where $X = \sigma_b/\sigma_1$ is the original ratio of the background light shot noise to the other noise sources before the coating is applied. The function F is plotted in Fig. 6. In the limit of large X, the reduction in noise is equal to the square root of the reduction in background light Y. In the limit of $X \to 0$, there is no improvement because the background light is an insignificant noise source.

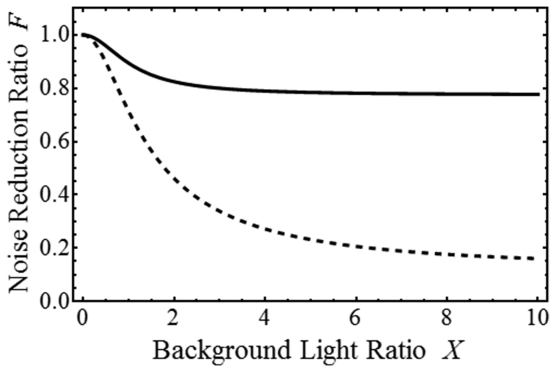

FIG. 6. The amount by which noise is reduced by a reduction in background light. Solid line—reduction by $Y = 0.6$; dashed line—reduction by $Y = 0.016$. X is the original magnitude of the noise from background light relative to other noise sources.

The two curves shown in Fig. 6 correspond to these two different cases, $Y = 0.60$ and $Y = 0.016$, and quantify the extent to which the application of the coating would reduce the noise coming from background light. The value of $Y = 0.60$ has been chosen to match the value measured in the experiment in Sec. III, rounded to two decimal places. The value of $Y = 0.016$ has been chosen to match the value measured in the reduction of 780 nm light in Fig. 3(b).

From Fig. 6, it can be seen that for a generalized cold atom sensor using a prism MOT and achieving the same background light suppression as achieved in Sec. III, a noise reduction of 23% is possible. This would present a significant improvement in an experimental system, with little increase in the overall complexity. It is worth noting that in addition to the improvements quantified in the above analysis, a sufficiently good coating material might reduce background scattered light to the extent that it is not necessary to use a background subtraction method at all, leading to further improvements.

Due to the vast variety in types of cold atom experiments, the vacuum chambers used are often bespoke to the experiment in question, consequently the exact angles at which background scattered light will reach the detector will be unique to the vacuum chamber and often will have undergone multiple reflections to reach the detector. By characterizing a coating BRDF at these angles and using Eq. (4), it should be possible to estimate the noise reduction possible in a specific system to estimate the noise reduction possible.

VI. CONCLUSION

The potential improvements of a reduction in background light levels were explored for cold atom systems. The optical properties of a coating were tested compared to a titanium surface, a common vacuum chamber material. The coating was found capable of reducing the peak scattered light by a factor of 62 at 780 nm providing a significant reduction in reflected light. The vacuum compatibility of the coating has been examined, and the outgassing has been found to be less than 3×10^{-8} mbar L cm^{-2} s^{-1}, where the measurement was limited by the vacuum chamber used. Outgassing at this level

and below means the coating is suitable for high vacuum applications, at pressures used in most cold atom experiments. The coating was then applied to a titanium vacuum chamber. Housed within this vacuum chamber are the optics required to produce a prism MOT, where the coating was observed to be nonreactive with rubidium. These properties make the coating suitable for use in cold atom systems.

Within the prism MOT, a reduction in background light by roughly 40% was observed, providing a significant improvement in a system prone to high background light levels from the vacuum chamber and the optical components used to form the MOT. The effect of achieving this background light reduction was then explored theoretically in a generalized cold atom sensor using a prism MOT. Based on the experimental results, a noise reduction of 23% was found to be possible, presenting a significant potential improvement.

The work presented here provides the experimental and theoretical tools needed to evaluate whether a low-reflectivity coating would offer an improvement in an existing cold atom system. The results from applying the low-reflectivity coating show great promise for the implementation of low-reflectivity vacuum compatible coatings as a way to achieve scattered light suppression when measuring fluorescence signals from gas-phase sources in cold atom systems.

ACKNOWLEDGMENTS

The authors would like to thank the University of Birmingham's Physics workshop team for machining the custom vacuum chambers used in these experiments. We would also like to thank Jonathan Bass for lending us some of the lasers used for the experiment shown in Fig. 2. The authors would like to acknowledge funding from EPSRC through Grant Nos. EP/M013294 and EP/S004084/1, DSTL through Contract No. DSTLX-1000095040, and Innovate UK through the Gravity Pioneer Grant No. 104613.

APPENDIX A: CHAMBER GEOMETRY AND CONSTRUCTION

The vacuum chamber design and dimensions of the vacuum used in these experiments can be seen in Fig. 7.

Teflon caps were used to protect the threaded holes and the knife-edge during the coating process [see Fig. 8(a)]. After coating, sealing surfaces were machined to provide flat surfaces for indium

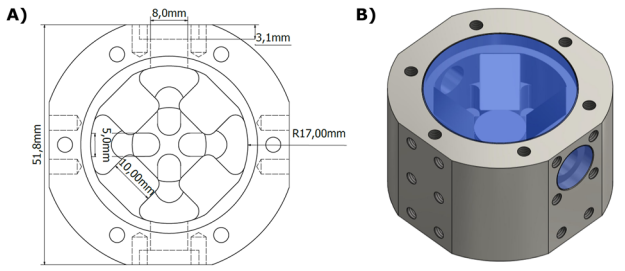

FIG. 7. (a) Diagram showing the vacuum chamber dimensions. (b) CAD model showing the assembled chamber.

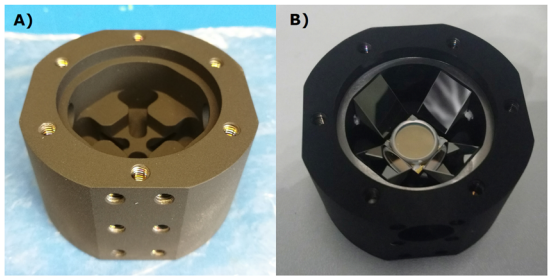

FIG. 8. (a) The prism MOT chamber post coating. (b) The chamber post machining and assembly of optical components.

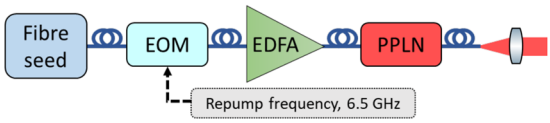

FIG. 9. Schematic of the laser used for optical trapping. The output light from a seed laser (1550 nm) is modulated by an EOM driven by a 6.5 GHz oscillator to generate frequency sidebands. The light is then amplified by an EDFA before being frequency doubled via second harmonic generation using a PPLN waveguide. The output of the fiber is allowed to expand, before being collimated using a lens. This collimated light is then input into the MOT vacuum chamber.

sealing the glass windows to the titanium chamber. Then, the prisms, the mirror, and the quarter wave plate were glued in place with a vacuum compatible glue. The chamber before the windows were attached can be seen in Fig. 8(b).

APPENDIX B: LASER SYSTEM FOR OPTICAL TRAPPING

The light used to cool and trap the atoms is generated using a fiber laser system, a schematic of which can be seen in Fig. 9. The two frequencies needed for cooling ^{87}Rb atoms on the D_2 transition are derived from the carrier and first-order frequency sideband created by phase modulation. The light from the seed laser is passed through an electro-optical modulator (EOM), which modulates the light at ~6.5 GHz to generate a sideband that acts as the repumping frequency on the $|F = 1\rangle \rightarrow |F' = 2\rangle$ transition, while the carrier acts as the cooling frequency on the cycling $|F = 2\rangle \rightarrow |F' = 3\rangle$ transition. The light is then amplified with an erbium-doped fiber amplifier (EDFA); then, a periodically poled lithium niobate (PPLN) waveguide is used to frequency double the light from 1560 nm to 780 nm. The light out of the fiber is then collimated before being used to trap atoms.

APPENDIX C: MEASURING ATOM NUMBER AND LOADING RATE

The number of atoms trapped and the loading rate in the prism MOT systems were measured using the method in Ref. 38. The MOT was loaded from background rubidium gas in the vacuum chamber, generated due to the use of the rubidium dispenser located close to the MOT region of the chamber. This pressure is typical in these sorts of systems, and often, a pressure gradient is present between the MOT region and the measurement region, with the measurement region being at a lower pressure.

DATA AVAILABILITY

The data that support the findings of this study are available from the corresponding author upon reasonable request.

REFERENCES

[1] A. Wicht, J. M. Hensley, E. Sarajlic, and S. Chu, "A preliminary measurement of the fine structure constant based on atom interferometry," Phys. Scr. **T102**, 82 (2002).

[2] A. Bonnin, N. Zahzam, Y. Bidel, and A. Bresson, "Characterization of a simultaneous dual-species atom interferometer for a quantum test of the weak equivalence principle," Phys. Rev. A **92**, 023626 (2015).

[3] J. B. Fixler, G. T. Foster, J. M. McGuirk, and M. A. Kasevich, "Atom interferometer measurement of the Newtonian constant of gravity," Science **315**, 74–77 (2007).

[4] S. Merlet, A. Kopaev, M. Diament, G. Geneves, A. Landragin, and F. Pereira Dos Santos, "Micro-gravity investigations for the LNE watt balance project," Metrologia **45**, 265–274 (2008).

[5] J. M. Hogan, D. M. S. Johnson, S. Dickerson, T. Kovachy, A. Sugarbaker, S.-w. Chiow, P. W. Graham, M. A. Kasevich, B. Saif, S. Rajendran, P. Bouyer, B. D. Seery, L. Feinberg, and R. Keski-Kuha, "An atomic gravitational wave interferometric sensor in low earth orbit (AGIS-LEO)," Gen. Relativ. Gravitation **43**, 1953–2009 (2011).

[6] J. M. Hogan and M. A. Kasevich, "Atom-interferometric gravitational-wave detection using heterodyne laser links," Phys. Rev. A **94**, 033632 (2016).

[7] S. Dimopoulos, P. W. Graham, J. M. Hogan, M. A. Kasevich, and S. Rajendran, "Atomic gravitational wave interferometric sensor," Phys. Rev. D **78**, 122002 (2008).

[8] K. Bongs, M. Holynski, J. Vovrosh, P. Bouyer, G. Condon, E. Rasel, C. Schubert, W. P. Schleich, and A. Roura, "Taking atom interferometric quantum sensors from the laboratory to real-world applications," Nat. Rev. Phys. **1**, 731–739 (2019).

[9] Y. Bidel, O. Carraz, R. Charrière, M. Cadoret, N. Zahzam, and A. Bresson, "Compact cold atom gravimeter for field applications," Appl. Phys. Lett. **102**, 144107 (2013).

[10] A. Hinton, M. Perea-Ortiz, J. Winch, J. Briggs, S. Freer, D. Moustoukas, S. Powell-Gill, C. Squire, A. Lamb, C. Rammeloo, B. Stray, G. Voulazeris, L. Zhu, A. Kaushik, Y.-H. Lien, A. Niggebaum, A. Rodgers, A. Stabrawa, D. Boddice, S. R. Plant, G. W. Tuckwell, K. Bongs, N. Metje, and M. Holynski, "A portable magneto-optical trap with prospects for atom interferometry in civil engineering," Philos. Trans. R. Soc., A **375**, 20160238 (2017).

[11] M. Meunier, I. Dutta, R. Geiger, C. Guerlin, C. L. Garrido Alzar, and A. Landragin, "Stability enhancement by joint phase measurements in a single cold atomic fountain," Phys. Rev. A **90**, 063633 (2014).

[12] I. Dutta, D. Savoie, B. Fang, B. Venon, C. L. Garrido Alzar, R. Geiger, and A. Landragin, "Continuous cold-atom inertial sensor with 1 nrad/sec rotation stability," Phys. Rev. Lett. **116**, 183003 (2016).

[13] Q. Hu, J. Yang, Y. Luo, A. Jia, F. Xu, C. Wei, and Q. Li, "Towards a juggling ^{87}Rb atomic dual fountain," AIP Adv. **8**, 035316 (2018).

[14] M. Langlois, R. Caldani, A. Trimeche, S. Merlet, and F. Pereira dos Santos, "Differential phase extraction in dual interferometers exploiting the correlation between classical and quantum sensors," Phys. Rev. A **96**, 053624 (2017).

[15] D. N. Aguilera, H. Ahlers, B. Battelier, A. Bawamia, A. Bertoldi, R. Bondarescu, K. Bongs, P. Bouyer, C. Braxmaier, L. Cacciapuoti, C. Chaloner, M. Chwalla, W. Ertmer, M. Franz, N. Gaaloul, M. Gehler, D. Gerardi, L. Gesa, N. Gürlebeck, J. Hartwig, M. Hauth, O. Hellmig, W. Herr, S. Herrmann, A. Heske, A. Hinton, P. Ireland, P. Jetzer, U. Johann, M. Krutzik, A. Kubelka, C. Lämmerzahl, A. Landragin, I. Lloro, D. Massonnet, I. Mateos, A. Milke, M. Nofrarias, M. Oswald, A. Peters, K. Posso-Trujillo, E. Rasel, E. Rocco, A. Roura, J. Rudolph, W. Schleich, C. Schubert, T. Schuldt, S. Seidel, K. Sengstock, C. F. Sopuerta, F. Sorrentino, D. Summers, G. M. Tino, C. Trenkel, N. Uzunoglu, W. von Klitzing, R. Walser, T. Wendrich, A. Wenzlawski, P. Weßels, A. Wicht, E. Wille, M. Williams, P. Windpassinger, and N. Zahzam, "STE-QUEST—Test of the universality of free fall using cold atom interferometry," Classical Quantum Gravity **31**, 115010 (2014).

[16] R. H. Parker, C. Yu, W. Zhong, B. Estey, and H. Müller, "Measurement of the fine-structure constant as a test of the standard model," Science **360**, 191–195 (2018).

[17] X. Wu, Z. Pagel, B. S. Malek, T. H. Nguyen, F. Zi, D. S. Scheirer, and H. Müller, "Gravity surveys using a mobile atom interferometer," Sci. Adv. **5**, eaax0800 (2019).

[18] S. Pollock, "Integrated magneto-optical traps for atom chips," Ph.D. thesis, Imperial College London, 2010.

[19] M. Vangeleyn, P. F. Griffin, E. Riis, and A. S. Arnold, "Single-laser, one beam, tetrahedral magneto-optical trap," Opt. Express **17**, 13601–13608 (2009).

[20] G. Hall, K. Liu, M. J. McAuliffe, C. F. Giese, and W. R. Gentry, "State-to-state vibrational excitation of I_2 in collisions with He," J. Chem. Phys. **81**, 5577–5585 (1984).

[21] A. Adibekyan, E. Kononogova, C. Monte, and J. Hollandt, "High-accuracy emissivity data on the coatings Nextel $8_{11\text{-}21}$, Herberts 1534, Aeroglaze Z_30_6 and Acktar fractal black," Int. J. Thermophys. **38**, 89 (2017).

[22] J. Lehman, C. Yung, N. Tomlin, D. Conklin, and M. Stephens, "Carbon nanotube-based black coatings," Appl. Phys. Rev. **5**, 011103 (2018).

[23] S. Zeidler, T. Akutsu, Y. Torii, and Y. Aso, "Measuring scattering light distributions on high-absorptive surfaces for stray-light reduction in gravitational-wave detectors," Opt. Express **27**, 16890–16910 (2019).

[24] E. B. Norrgard, N. Sitaraman, J. F. Barry, D. J. McCarron, M. H. Steinecker, and D. DeMille, "In-vacuum scattered light reduction with black cupric oxide surfaces for sensitive fluorescence detection," Rev. Sci. Instrum. **87**, 053119 (2016).

[25] S. Xu, Y. Yin, R. Gu, M. Xia, L. Xu, L. Chen, Y. Xia, and J. Yin, "Note: Sensitive fluorescence detection through minimizing the scattering light by anti-reflective nanostructured materials," Rev. Sci. Instrum. **89**, 046103 (2018).

[26] T. Akutsu, Y. Saito, Y. Sakakibara, Y. Sato, Y. Niwa, N. Kimura, T. Suzuki, K. Yamamoto, C. Tokoku, S. Koike, D. Chen, S. Zeidler, K. Ikeyama, and Y. Ariyama, "Vacuum and cryogenic compatible black surface for large optical baffles in advanced gravitational-wave telescopes," Opt. Mater. Express **6**, 1613–1626 (2016).

[27] See www.sura-instruments.de for Sura Instruments; accessed 22 July 2019.

[28] H. J. Patrick, L. M. Hanssen, J. Zeng, and T. A. Germer, "BRDF measurements of graphite used in high-temperature fixed point blackbody radiators: A multi-angle study at 405 nm and 658 nm," Metrologia **49**, S81 (2012).

[29] L.-P. Sung, M. E. Nadal, M. E. McKnight, E. Marx, and B. Laurenti, "Optical reflectance of metallic coatings: Effect of aluminum flake orientation," J. Coat. Technol. **74**, 55–63 (2002).

[30] J. S. Gondek, G. W. Meyer, and J. G. Newman, "Wavelength dependent reflectance functions," in *Proceedings of the 21st Annual Conference on Computer Graphics and Interactive Techniques, SIGGRAPH '94* (ACM, New York, NY, USA, 1994), pp. 213–220.

[31] M. Taborelli, "Cleaning and surface properties," in *CERN Accelerator School, course on Vacuum in Accelerators, Platja d'Aro, Spain, 16–24 May 2006* (CERN, 2006), pp. 321–324.

[32] R. Grinham and A.Chew, "A review of outgassing and methods for its reduction," Appl. Sci. Convergence Technol. **26**, 95–109 (2017).

[33] P. A. Redhead, "Ultrahigh vacuum pressure measurements: Limiting processes," J. Vac. Sci. Technol., A **5**, 3215–3223 (1987).

[34] J. C. Camparo, R. P. Frueholz, and B. Jaduszliwer, "Alkali reactions with wall coating materials used in atomic resonance cells," J. Appl. Phys. **62**, 676–681 (1987).

[35] J. Dalibard and C. Cohen-Tannoudji, "Laser cooling below the Doppler limit by polarization gradients: Simple theoretical models," J. Opt. Soc. Am. B **6**, 2023–2045 (1989).

[36] E. L. Raab, M. Prentiss, A. Cable, S. Chu, and D. E. Pritchard, "Trapping of neutral sodium atoms with radiation pressure," Phys. Rev. Lett. **59**, 2631–2634 (1987).

[37] A. Yariv, *Optical Electronics*, 3rd ed. (Holt, Reinhart and Winston, 1985).

[38] R. W. G. Moore, L. A. Lee, E. A. Findlay, L. Torralbo-Campo, G. D. Bruce, and D. Cassettari, "Measurement of vacuum pressure with a magneto-optical trap: A pressure-rise method," Rev. Sci. Instrum. **86**, 093108 (2015).